Permittivity Gradient Induced Depolarization: Electromagnetic Propagation With the Maxwell Vector Wave Equation

Stephen R. Shaffer and Alex Mahalov

***Abstract*— Recent interest in 3-D vectorial sensors requires the development of vectorial propagation methods, rather than scalar wave equation approaches. We derive a vector wave equation from Maxwell's equations for a medium which has an inhomogeneous dielectric permittivity dominated by variation along one dimension. It is well known that the electric field components decouple for homogeneous media. However, 1-D permittivity variations yield an upper triangular system of scalar wave equations with the wave polarization component parallel to the inhomogeneous direction/axis acting as a forcing term for the orthogonal components. The main implication is that waves with polarization oriented parallel to the permittivity gradient will act as a forcing term and excite other polarization components and, thus, induce depolarization. Contemporary studies treat the permittivity as a constant when deriving a wave equation or paraxial approximation, and then re-introduce via inhomogeneous wave speed, variable permittivity, thus missing important terms and physical mechanisms in their resulting equations. Contemporary studies neglect the term in the Maxwell vector wave equation responsible for this effect. Application of the electromagnetic propagation depolarization effect is demonstrated numerically for an air–sea interface evaporation duct with a 500 MHz source.**

***Index Terms*— Electromagnetic (EM) propagation, nonhomogeneous media.**

I. Introduction, Background, and Motivation

ELECTROMAGNETIC (EM) propagation in inhomogeneous media poses several challenges and there is a need to go beyond standard scalar propagation models based on scalar wave, Helmholtz, and paraxial equations and to incorporate vector wave propagation effects. Contemporary studies treat the permittivity as a constant when deriving a scalar wave equation or paraxial approximation. Mohsen [1] considers the electromagnetic field within a stationary nonconducting source-free medium which satisfies the stationary Maxwell equations. A solution for the field is given in terms of the two Hertz vectors for a general orthogonal coordinate system. In the context of geometric optics, McDaniel and Mahalov [2], [3] studied the impacts of refractive index gradients on electromagnetic propagation in random media. It is well known that the electric field components decouple for homogeneous media. It has also been well established since, e.g., [4], [5], that homogeneous turbulent media causes polarization fluctuations, which [6] shows to have a λ^2 dependence and is negligible for the optical regime but suggest may be important for longer wavelengths. Despite this suggestion, contemporary studies which proceeded for longer wavelengths retained the assumption of neglecting this effect [7].

Our work is grounded in a first-principle approach, beginning with the fundamental vector Maxwell equations. By retaining gradients of the refractive index in the derivation of the Maxwell vector wave equation (MVWE), we capture depolarization effects as a result. We show that 1-D anisotropic permittivity variations yield an upper triangular system of wave equations, with the component parallel to the inhomogeneous direction/axis acting as a forcing term for the orthogonal components of the electric field. The main implication is that waves with polarization oriented parallel to the inhomogeneous dimension will excite other polarization components, inducing depolarization.

There are many recent areas of inquiry for which a more comprehensive vectorial theory could find the application. The eigenvalue problem for the MVWE was considered by [8] stressing the mathematical challenges of the vector problem in contrast with the scalar problem, which remains an active area of research [9], [10]. The importance of vector cross-polarization effects is discussed in [11] and [12]. The term responsible for depolarization is retained by [13]–[15], where they discuss orbital angular momentum and other effects. Polarized inertial gravity wave excitations give rise to Rayleigh–Taylor organizing mixing patterns within ionospheric plasma flows, where accumulation enhances media inhomogeneities inducing large density and, thus, permittivity gradients [16]–[20], which may, thus, influence transionospheric propagation and communication. There are also ground-based remote observations of 3-D structures in the ionosphere [21], magnetosphere propagation experiments [22], detecting 3-D wave vector components [23], and full-wave 3-D propagation modeling [24], which could be extended by our method—and additional generalization, to incorporate depolarization for fully anisotropic media.

Manuscript received March 17, 2020; revised June 23, 2020; accepted July 21, 2020. Date of publication August 19, 2020; date of current version March 3, 2021. This work was supported by the Air Force Office of Scientific Research under Grant FA9550-19-1-0064. *(Corresponding author: Stephen R. Shaffer.)*

The authors are with the School of Mathematical and Statistical Sciences, Arizona State University, Tempe, AZ 85287-1804 USA (e-mail: stephen.shaffer@asu.edu; mahalov@asu.edu).

Digital Object Identifier 10.1109/TAP.2020.3016463

Novel 3-D vector sensor technologies require the development of vector EM propagation models derived from the fundamental Maxwell equations [23]. *In situ* CubeSat satellite missions are being developed with novel vector antenna technology which is anticipated to be a pathfinder for future swarms of in-space interferometric radio telescopes [23], [25], [26]. Interferometric observations may encounter differential depolarization depending upon observation baseline and local structure of medium inhomogeneities. Applications for 3-D vector sensors include observing ionosphere and space weather, solar radio burst emissions, plasma waves, and radiation in the heliosphere [27]. Synthetic radio observations of stellar coronal radio emissions [28] and propagation through space weather in stellar environments will also be influenced by permittivity gradient-based depolarization [29]. Astronomical signals, such as observed with low-frequency radio arrays for extra-galactic sources, may depolarize along their entire path and in the last moments of their journey to the detector [30].

Terrestrial applications include EM propagation in evaporation ducts, which are a downward refracting layer that results from the rapid decrease in humidity with respect to altitude occurring in the atmospheric surface layer above bodies of water or clouds. Characteristics of evaporation ducts were studied extensively in the coupled air–sea processes and electromagnetic ducting research (CASPER) campaigns [31]. The boundary layer phenomenon of evaporation ducts has land-based analogs, for which scintillometry has been employed for urban [32]–[35] and agricultural [36] applications. Sand and dust storms also cause cross polarization, as discussed by [37]. Studies on atmospheric propagation include quantifying refractivity from propagation loss [38]. There are also engineering applications for materials to manipulate guided surface waves within varying dielectric materials for cloaking purposes [39] and for synthetic aperture radar [40]. Dual-polarization techniques used in communication via dual-polarization frequency reuse, e.g., [41], or observations of hydrometers, e.g., [42], also need to account for signal depolarization.

II. Derivation of MVWE Governing Equations From Maxwell's Equations

We derive a vector wave equation from Maxwell's equations

$$\nabla \cdot \mathbf{D} = \rho \tag{1}$$

$$\nabla \cdot \mathbf{B} = 0 \tag{2}$$

$$\frac{\partial \mathbf{B}}{\partial t} = -\nabla \times \mathbf{E} \tag{3}$$

$$\frac{\partial \mathbf{D}}{\partial t} = \nabla \times \mathbf{H} - \mathbf{J} \tag{4}$$

for a medium which has an inhomogeneous dielectric permittivity dominated by variation along one dimension. The electric displacement and magnetic fields are, $\mathbf{D} = \epsilon\mathbf{E} + \mathbf{P}$, and $\mathbf{H} = \mu_0^{-1}\mathbf{B} - \mathbf{M}$, respectively, given in terms of electric field ($\mathbf{E}$), electric polarization ($\mathbf{P}$), magnetic induction ($\mathbf{B}$), and magnetic polarization ($\mathbf{M}$), respectively. Here, μ_0 is the magnetic permeability, a constant, and ϵ is the electric permittivity, dependent upon medium properties. We first derive the general vector wave equation and then apply restrictions to a specific cause for our study. Taking the curl of Faraday's Law (3), using the vector identity $\nabla \times \nabla \times \mathbf{A} = \nabla(\nabla \cdot \mathbf{A}) - \Delta\mathbf{A}$, with a fixed magnetic permiability μ_0, and then using Ampére's law (4), gives, respectively

$$\nabla \times \frac{\partial \mu_0(\mathbf{H} + \mathbf{M})}{\partial t} = -\nabla \times \nabla \times \mathbf{E} = \Delta\mathbf{E} - \nabla(\nabla \cdot \mathbf{E}) \tag{5}$$

$$\frac{\partial}{\partial t}\mu_0\left(\frac{\partial}{\partial t}(\epsilon\mathbf{E}) + \mathbf{P} + \mathbf{J} + \nabla \times \mathbf{M}\right) = \Delta\mathbf{E} - \nabla(\nabla \cdot \mathbf{E}). \tag{6}$$

Rearranging Coulomb's law (1) as

$$\nabla \cdot \mathbf{E} = \epsilon^{-1}(\rho - \nabla\epsilon \cdot \mathbf{E} - \nabla \cdot \mathbf{P}) \tag{7}$$

and substituting into (6), we arrive at an MVWE

$$\frac{\partial}{\partial t}\mu_0\left(\frac{\partial}{\partial t}(\epsilon\mathbf{E}) + \mathbf{P} + \mathbf{J} + \nabla \times \mathbf{M}\right) = \Delta\mathbf{E} - \nabla(\epsilon^{-1}(\rho - \nabla\epsilon \cdot \mathbf{E} - \nabla \cdot \mathbf{P})). \tag{8}$$

For our study, we consider an unpolarized medium ($\mathbf{P} = \vec{0}$) without an applied magnetic field ($\mathbf{M} = \vec{0}$) and no charges ($\rho = 0$) or current ($\mathbf{J} = \vec{0}$). These restrictions yield the MVWE for $\mathbf{E}$

$$\frac{\partial}{\partial t}\mu_0\frac{\partial}{\partial t}(\epsilon\mathbf{E}) - \Delta\mathbf{E} - \nabla(\epsilon^{-1}\nabla\epsilon \cdot \mathbf{E}) = 0. \tag{9}$$

The third term in (9) is responsible for depolarization effects and is often neglected by omission of the second term on the right-hand side of (7) when assuming $\nabla\epsilon = 0$ as in many contemporary studies. In the following, we describe $\epsilon^{-1}\nabla\epsilon$ in terms of an inverse length scale for variations of the media.

With $\mu = \mu_0$ a constant and allowing only one dominant dimension of permittivity variation, we begin restricting the general case given by (9) to our specific study. We use a right-handed Cartesian coordinate system such that the permittivity variation aligns with $\hat{x_3}$, i.e., $\epsilon = \epsilon(x_3)$, e.g., due to a permittivity gradient layer, described in the following for the application of an evaporation duct (Fig. 1). The operators for the gradient and Laplacian have their usual Cartesian form (see Appendix). This choice yields the following equation:

$$\mu_0\frac{\partial^2\epsilon\mathbf{E}}{\partial t^2} - \Delta\mathbf{E} - \nabla(\alpha E_3) = 0. \tag{10}$$

Here

$$\alpha = \alpha(x_3) = \epsilon^{-1}(x_3)\frac{\partial\epsilon(x_3)}{\partial x_3} = \frac{\partial}{\partial x_3}\ln\epsilon(x_3) = L_\epsilon^{-1} \tag{11}$$

where $L_\epsilon = \alpha^{-1}$ is a length scale characterizing inhomogeneous media for the electric permittivity gradient layer. Observe that (10) is a homogeneous equation and that a forcing, as by an antenna, can be incorporated by setting the right-hand side to a nonzero function [43], [44].

The wave equation (10) is equivalent to the upper triangular system of equations for each component of **E**

$$\mu_0\epsilon\frac{\partial^2 E_1}{\partial t^2} - \Delta E_1 - \alpha(x_3)\frac{\partial E_3}{\partial x_1} = \mathcal{F}_H(t, x_1, x_3)\delta(x_2 - x_T) \tag{12}$$

$$\mu_0\epsilon\frac{\partial^2 E_2}{\partial t^2} - \Delta E_2 - \alpha(x_3)\frac{\partial E_3}{\partial x_2} = 0 \tag{13}$$

$$\mu_0\epsilon\frac{\partial^2 E_3}{\partial t^2} - \Delta E_3 - \frac{\partial \alpha(x_3) E_3}{\partial x_3} = \mathcal{F}_V(t, x_1, x_3)\delta(x_2 - x_T). \tag{14}$$

The forcing terms $\mathcal{F}()$ are included here to represent a transmitter at range position x_T, for transmitters which are either vertically polarized along $\hat{x}_3$, $\mathcal{F}_V()$, or horizontally polarized along $\hat{x}_1$, $\mathcal{F}_H()$. Elliptically polarized sources could be handled by controlling the relative amplitudes and phases of $\mathcal{F}_H()$ and $\mathcal{F}_V()$, but only a vertically polarized source will be considered in the present study.

III. Evaporation Duct Application

A. Layered Media Permittivity Profile, $\epsilon = \epsilon(x_3)$

The present work will be applied to evaporation ducts, an ubiquitous phenomenon of the marine atmospheric surface layer, where the refractive index changes rapidly due to humidity above the air–sea interface. The CASPER project [31], [45], [46] describes sea spray and other factors influencing the permittivity gradient. A basic modified refractivity profile for characterizing radar propagation can be estimated from observable atmospheric thermodynamic properties, as given by [31], that is

$$M = \frac{77.6}{T}\left(p + 4810\frac{e}{T}\right) + \frac{z}{R} \times 10^6 \tag{15}$$

with T temperature [K], p atmospheric pressure [hPa], e water vapor pressure [hPa], z height above mean sea level (MSL) [m], R mean radius of Earth [m]. The last term accounts for Earth's curvature. Ducting occurs in the near-surface layer where $dM/dz < 0$. Monin Obukhov Similarity Theory scaling relationships are often employed for empirically estimating T and e, with many caveats as discussed by [31]. Evaporation duct height, typically around 10–50 m, and can extend up to 2 km above MSL, as determined from the height of the minimum value of M from the near-surface profile, which is dominated by variations in humidity gradients within the surface layer [46]. The relationship between M units and permittivity is given by

$$M = 10^6(n-1) = 10^6\left(\epsilon_r^2 - 1\right) = 10^6\left(\epsilon^2\epsilon_0^{-2} - 1\right) \tag{16}$$

with ϵ_r being the relative permittivity and ϵ_0 the vacuum permittivity.

We define a right-handed Cartesian coordinate system such that the unit vector $\hat{x}_3$ is orthogonal to the mean air–sea interface and parallel to a vertically polarized source, $\mathcal{F}_V(\cdot)$, and $\hat{x}_1$ is parallel to a horizontally polarized source, $\mathcal{F}_H(\cdot)$. We are neglecting air–water interface waves and associated scattering complexities for the present study. We set $\hat{x}_2$ to be oriented along the initial path of signal propagation from a stationary transmitter to a receiver, before refractive effects may influence the propagation direction, as shown in Fig. 1.

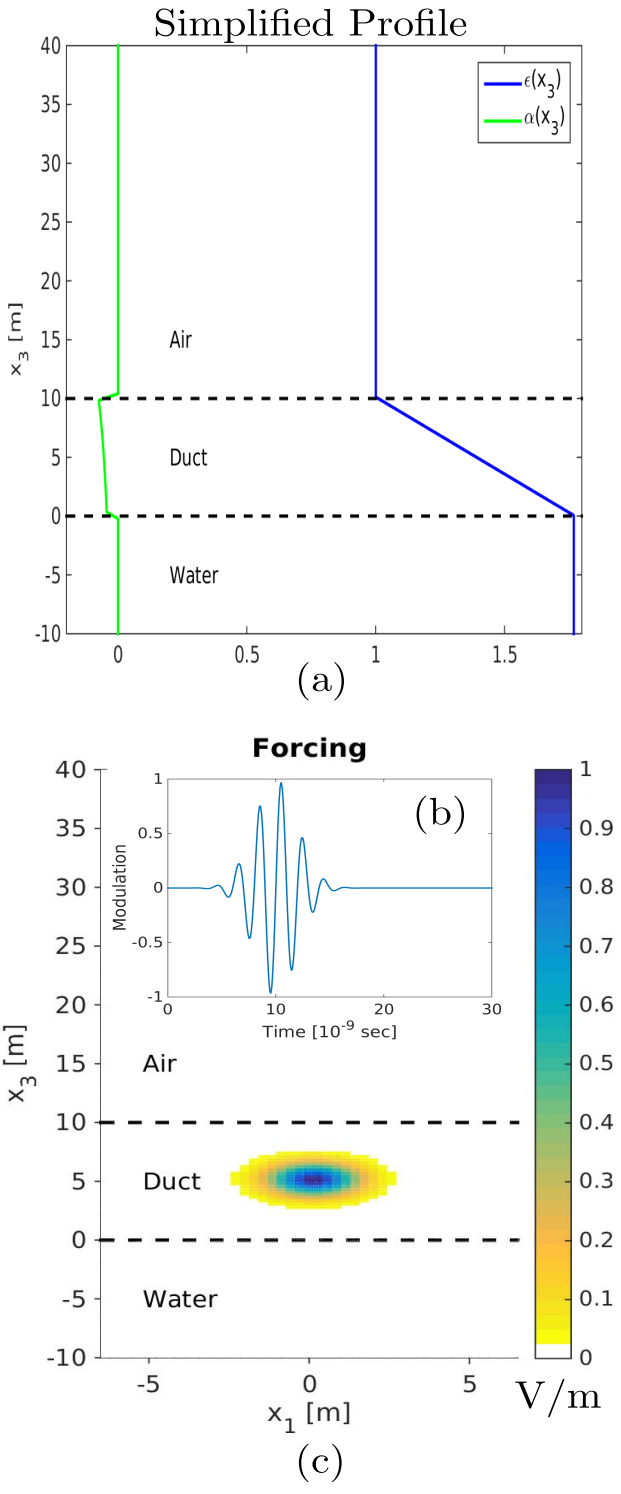

Fig. 1. (a) Vertical profiles of electric permittivity $\epsilon(x_3)$ given by (17) (blue) and $\alpha(x_3)$ given by (11) (green) for the simplified linear ramp (17) approximation of the evaporation duct ("duct") at the air–sea interface (neglecting air–water interface waves). For comparison with observed profiles (in M-units), refer to [45, Fig. 14]. (b) Forcing function modulation timeseries, temporal part of (18). (c) Vertical cross section in the x_1-x_3 plane of the maximum spatial part of the forcing function (18), $\max \mathcal{F}_V(t, x_1, x_3)\delta(x_2 - x_T)$, used in (14), to show the transmitter beam shape function. A right-handed Cartesian coordinate system is used and $\hat{x}_2$ is directed into the page.

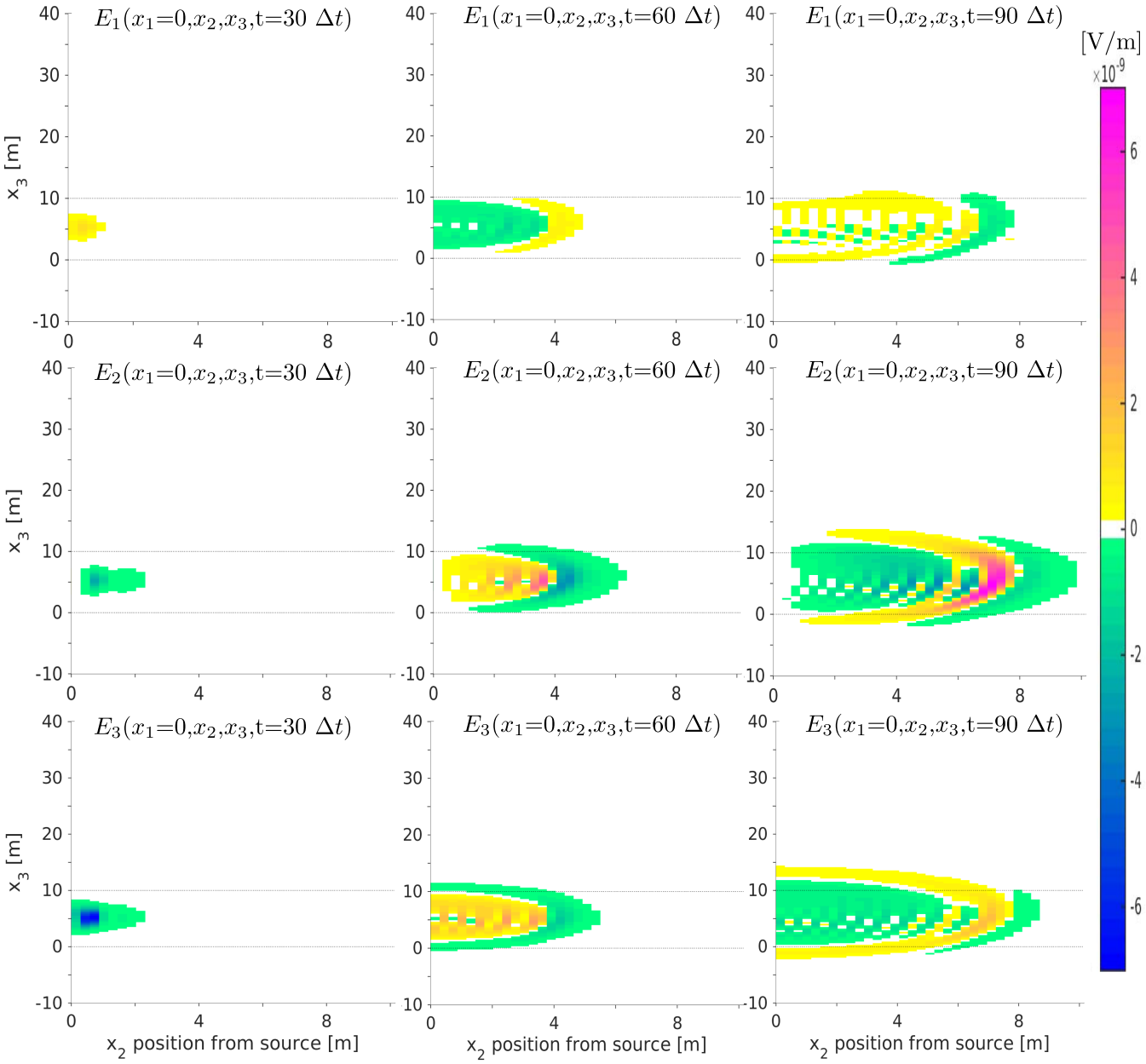

Fig. 2. Vertical cross section on source optical plane ($x_1 = 0$) of electric field components E_1 (top) E_2 (middle) and E_3 (bottom) at different snapshots of time. Case $\epsilon(x_3)$ as in (17). Both refraction and depolarization effects are apparent. Here, we see E_2 is more strongly forced than E_1 for this configuration. Horizontal dotted line indicates extent of $\alpha \neq 0$ as in Fig. 1.

As a simplifying approximation to (15) and (16), we use a linear ramp profile, as shown in Fig. 1(a), given by

$$\epsilon(x_3) = \begin{cases} \epsilon_0 n_l^2, & x_3 < 0 \\ \epsilon_0 \dfrac{n_u^2 - n_l^2}{\Lambda} x_3 + \epsilon_0 n_l^2, & 0 \le x_3 \le \Lambda \\ \epsilon_0 n_u^2, & x_3 > \Lambda. \end{cases} \tag{17}$$

Here, the duct height is given by Λ (we set $\Lambda = 10$ m), and lower/upper values of refractive index are given by $n_l = 1.33$ (water) and $n_u = 1 + 353.1 \times 10^{-6}$ (air at wavenumber 29.1 cm^{-1}) [47], respectively.

B. Antenna Forcing Function and Boundary Conditions

A simplified Gaussian modulated source, see Fig. 1(b), is used to represent antenna forcing in the systems (12)–(14). A pulse duration of $D = 10$ periods for a continuous wave (CW) source with frequency $f = 500$ MHz was chosen. The forcing beam pattern [Fig. 1(c)] has a Gaussian cross section centered at $(x_1, x_2, x_3) = (0, x_T, x_{3,s} = 5\ \mathrm{m})$ with half-width

(3 dB beamwidth) $L = 1$ m, given by

$$\mathcal{F}_V(t, x_1, x_3) = E_{3,\max} \sin(2\pi f t) \exp\left(\frac{-(t - \frac{D}{2f})^2}{2(D/10f)^2}\right) \times \exp\left(\frac{-\sqrt{2\ln 2}}{2L}(x_1^2 + (x_3 - x_{3,s})^2)\right). \tag{18}$$

Fig. 1(b) shows the time series of the $\mathcal{F}_V(t, x_1 = 0, x_2 = x_T, x_3 = 5)$ and a vertical cross section of $\max \mathcal{F}_V(t, x_1, x_2 = x_T, x_3)$ is shown in Fig. 1(c). We set $E_{3,\max} = 1$ V m^{-1}.

For the present study, we adopt the zero boundary conditions which fully reflect waves at the boundary, rather than employing a perfectly matched layer or other absorbing boundary conditions, which were developed for the curl system and near-normal incidence [48]. This choice was motivated by the phenomena of depolarization being strictly an interior problem, and we want to avoid conflating these dynamics with boundary condition issues. By limiting the simulation duration to before the pulse reflects from the boundary, we avoid unphysical issues of the choice of boundary condition. The domain is taken to be a rectangular box with dimensions 40 m $\times$ 40 m $\times$ 50 m, centered in x_1-x_2 at the transmitter position, as shown in Fig. 1, with the right half-space shown in Fig. 2. A numerical approach based upon a Yee scheme [49] is employed and is described in the Appendix.

IV. Results and Discussion

Depolarization will be measured as the ratio of complex electric field of the wave orthogonally polarized to the transmitted wave (E_d) to that copolarized (E_c) with the transmitted wave (E_t), given by

$$D = E_d / E_c \tag{19}$$

as per [50]. For our case, $E_t = E_c = E_3$, and $E_d = \text{span}\{E_1, E_2\}$. Fig. 2 shows several EM propagation model output times for vertical cross sections of E_1, E_2, and E_3, along the optical axis in the direction of propagation. Depolarization is apparent in Fig. 2, where E_1 and E_2 are nonzero, and thus, $D \neq 0$. Furthermore, the signal depolarization which occurs within the permittivity gradient layer is shown to propagate out of that layer.

There are many settings for which broader impacts and implications of these results for EM propagation experiencing electromagnetic ducting are anticipated, e.g., ionosphere electron density and marine atmospheric boundary layer evaporation ducts, as example environments which have anisotropic permittivity gradients with length scales comparable to the EM wavelength ($L_\epsilon \sim \lambda$). Depolarization from inhomogeneous permittivity should be considered for transionospheric propagation, variations due to ionosphere/space weather, solar radio burst emissions, plasma waves and radiation in the heliosphere, and so on. Recent developments in vector sensor technology require full vector propagation model capabilities based upon 3-D vector Maxwell equations coupled wave equations. Vectorial sensors can be used to measure depolarization forcing between electric field components of polarized waves. Furthermore, these results indicate that vector sensor interferometry needs to consider variations of depolarization along different propagation paths from inhomogeneous gradients of permittivity.

V. Conclusion

Electromagnetic propagation in inhomogeneous media with an anisotropic permittivity gradient exhibits depolarization effects through a coupling of EM wave components as demonstrated with a numerical model. Conventional EM wave propagation methods based upon scalar wave/Helmholtz/paraxial equation techniques do not capture depolarization effects in inhomogeneous media. Without coupling, a constant permittivity profile will not cause depolarization (not shown). Inhomogeneous/anisotropic media, such as the layered media examined here (i.e., $\epsilon = \epsilon(x_3)$), give rise to an upper triangular system not a scalar equation. A scalar equation propagates only the individual electric field components without coupling. In the upper-triangular system, the electric field component parallel to the inhomogeneous direction is a forcing term for the orthogonal components when $\alpha = \epsilon^{-1}\nabla\epsilon \neq 0$. A source initially linearly polarized parallel to the inhomogeneous direction will depolarize, and the received signal will have nonzero orthogonal components (i.e. E3-polarized source and $\epsilon(x_3)$ anisotropy will develop nonzero E_1 and E_2 components). We have shown that EM waves with linear polarization oriented parallel to the inhomogeneous direction of an anisotropic media excite orthogonal polarization components.

Appendix

A. System Equations and 3-D FDTD Numerical Scheme

Consider a 3-D domain. The components of the electric field vector are expressed as

$$E_j = E_j(t, x_1, x_2, x_3), \quad j = 1, 2, 3. \tag{20}$$

The systems (12)–(14) can be written as

$$\mu_0\epsilon\frac{\partial^2 E_1}{\partial t^2} - \left(\frac{\partial^2}{\partial {x_1}^2} + \frac{\partial^2}{\partial {x_2}^2} + \frac{\partial^2}{\partial {x_3}^2}\right) E_1 - \alpha(x_3)\frac{\partial E_3}{\partial x_1} = \mathcal{F}_H(t, x_3)\delta(x_2 - x_T) \tag{21}$$

$$\mu_0\epsilon\frac{\partial^2 E_2}{\partial t^2} - \left(\frac{\partial^2}{\partial {x_1}^2} + \frac{\partial^2}{\partial {x_2}^2} + \frac{\partial^2}{\partial {x_3}^2}\right) E_2 - \alpha(x_3)\frac{\partial E_3}{\partial x_2} = 0 \tag{22}$$

$$\mu_0\epsilon\frac{\partial^2 E_3}{\partial t^2} - \left(\frac{\partial^2}{\partial {x_1}^2} + \frac{\partial^2}{\partial {x_2}^2} + \frac{\partial^2}{\partial {x_3}^2}\right) E_3 - \frac{\partial(\alpha(x_3)E_3)}{\partial x_3} = \mathcal{F}_V(t, x_3)\delta(x_2 - x_T). \tag{23}$$

A numerical scheme adapted from a Yee scheme [49] for a Cartesian grid, where $t = n\Delta t$, $x_1 = k\Delta x_1$, $x_2 = l\Delta x_2$, and $x_3 = m\Delta x_3$, with $k, l, m, n \in \mathbb{N}$. For simplicity, we set $\Delta x_j = \Delta x$, $j = 1, 2, 3$, and specify grid increments viz $\Delta x = (rf\sqrt{\mu_0\epsilon_{\max}})^{-1}$, with r being a resolution/sampling parameter, where $r = 2$ satisfies Nyquist criteria and, e.g., $r = 10$ uses ten grid-points per wavelength, shows numerical

convergence. The CW source/forcing frequency is specified by f, and $\epsilon_{\max} = \max \epsilon(x_3)$ ensures the grid spacing is based upon the shortest wavelength in the domain. To satisfy CFL conditions, we then set $\Delta t = \Delta x/(2c_0)$. The numerical scheme for the system of equations is, thus, written as

$$\begin{aligned} E_1|_{k,l,m}^{n+1} &= 2E_1|_{k,l,m}^{n} - E_1|_{k,l,m}^{n-1} + \frac{\Delta t^2}{\mu_0 \epsilon} \\ &\times \Big[+ \Delta x_1^{-2}\big(E_1|_{k+1,l,m}^{n} - 2E_1|_{k,l,m}^{n} + E_1|_{k-1,l,m}^{n}\big) \\ &+ \Delta x_2^{-2}\big(E_1|_{k,l+1,m}^{n} - 2E_1|_{k,l,m}^{n} + E_1|_{n,l-1,m}^{k}\big) \\ &+ \Delta x_3^{-2}\big(E_1|_{k,l,m+1}^{n} - 2E_1|_{k,l,m}^{n} + E_1|_{k,l,m-1}^{n}\big) \\ &+ (2\Delta x_3)^{-1}(\alpha|_{m+1} - \alpha|_{m-1})E_3|_{k,l,m}^{n} \\ &+ (2\Delta x_1)^{-1}\alpha|_{m}\big(E_3|_{k+1,l,m}^{n} - E_3|_{k-1,l,m}^{n}\big) \\ &+ \mathcal{F}_H|_{k,l=l_T,m}^{n}\Big] \end{aligned} \tag{24}$$

$$\begin{aligned} E_2|_{k,l,m}^{n+1} &= 2E_2|_{k,l,m}^{n} - E_2|_{k,l,m}^{n-1} + \frac{\Delta t^2}{\mu_0 \epsilon} \\ &\times \Big[+ \Delta x_2^{-2}\big(E_2|_{k+1,l,m}^{n} - 2E_2|_{k,l,m}^{n} + E_2|_{k-1,l,m}^{n}\big) \\ &+ \Delta x_2^{-2}\big(E_2|_{k,l+1,m}^{n} - 2E_2|_{k,l,m}^{n} + E_2|_{k,l-1,m}^{n}\big) \\ &+ \Delta x_3^{-2}\big(E_2|_{k,l,m+1}^{n} - 2E_2|_{k,l,m}^{n} + E_2|_{k,l,m-1}^{n}\big) \\ &+ \alpha|_{m}(2\Delta x_2)^{-1}\big(E_3|_{k,l+2,m}^{n} - E_3|_{k,l-2,m}^{n}\big)\Big] \end{aligned} \tag{25}$$

and

$$\begin{aligned} E_3|_{k,l,m}^{n+1} &= 2E_3|_{k,l,m}^{n} - E_3|_{k,l,m}^{n-1} + \frac{\Delta t^2}{\mu_0 \epsilon} \\ &\times \Big[+ \Delta x_2^{-2}\big(E_3|_{k+1,l,m}^{n} - 2E_3|_{k,l,m}^{n} + E_3|_{k-1,l,m}^{n}\big) \\ &+ \Delta x_2^{-2}\big(E_3|_{k,l+1,m}^{n} - 2E_3|_{k,l,m}^{n} + E_3|_{k,l-1,m}^{n}\big) \\ &+ \Delta x_3^{-2}\big(E_3|_{k,l,m+1}^{n} - 2E_3|_{k,l,m}^{n} + E_3|_{k,l,m-1}^{n}\big) \\ &+ (2\Delta x_3)^{-1}(\alpha|_{m+1} - \alpha|_{m-1})E_3|_{k,l,m}^{n} \\ &+ \alpha|_{m}(2\Delta x_3)^{-1}\big(E_3|_{k,l,m+1}^{n} - E_3|_{k,l,m-1}^{n}\big) \\ &+ \mathcal{F}_V|_{k,l=l_T,m}^{n}\Big]. \end{aligned} \tag{26}$$

REFERENCES

[1] A. Mohsen, "Electromagnetic field representation in inhomogeneous anisotropic media," *Appl. Phys.*, vol. 2, no. 3, pp. 123–128, Sep. 1973, doi: 10.1007/BF00883972.

[2] A. McDaniel and A. Mahalov, "Lensing effects in a random inhomogeneous medium," *Opt. Express*, vol. 25, no. 23, pp. 28157–28166, Nov. 2017. [Online]. Available: https://doi.org/10.1364/OE.25.028157

[3] A. Mcdaniel and A. Mahalov, "Stochastic mirage phenomenon in a random medium," *Opt. Lett.*, vol. 42, no. 10, pp. 2002–2005, May 2017, doi: 10.1364/OL.42.002002.

[4] V. Tatarskii, *Wave Propagation in a Turbulent Medium*. New York, NY, USA: McGraw-Hill, 1961.

[5] H. Hodara, "Laser wave propagation through the atmosphere," *Proc. IEEE*, vol. 54, no. 3, pp. 368–375, Mar. 1966, doi: 10.1109/PROC.1966.4698.

[6] J. Strohbehn and S. Clifford, "Polarization and angle-of-arrival fluctuations for a plane wave propagated through a turbulent medium," *IEEE Trans. Antennas Propag.*, vol. AP-15, no. 3, pp. 416–421, May 1967, doi: 10.1109/TAP.1967.1138937.

[7] J. W. Goodman, *Statistical Optics*. New York, NY, USA: Wiley, 1985. [Online]. Available: https://cds.cern.ch/record/789128

[8] D. Colton, P. Monk, and J. Sun, "Analytical and computational methods for transmission eigenvalues," *Inverse Problems*, vol. 26, no. 4, Mar. 2010, Art. no. 045011, doi: 10.1088/0266-5611/26/4/045011.

[9] F. Cakoni, O. Ivanyshyn Yaman, R. Kress, and F. Le Louër, "A boundary integral equation for the transmission eigenvalue problem for Maxwell equation," *Math. Methods Appl. Sci.*, vol. 41, no. 4, pp. 1316–1330, 2018. [Online]. Available: https://onlinelibrary.wiley.com/doi/abs/10.1002/mma.4664

[10] F. Cakoni, D. Colton, and P. Monk, "Qualitative methods in inverse electromagnetic scattering theory: Inverse scattering for anisotropic Media," *IEEE Antennas Propag. Mag.*, vol. 59, no. 5, pp. 24–33, Oct. 2017, doi: 10.1109/MAP.2017.2731662.

[11] L. Keefe, I. Zilberter, and T. J. Madden. (2018). *When Parabolized Propagation Fails: A Matrix Square Root Propagator for EM Waves*. [Online]. Available: https://arc.aiaa.org/doi/abs/10.2514/6.2018-3113

[12] D. Rogers, "Propagation considerations for satellite broadcasting at frequencies above 10 GHz," *IEEE J. Sel. Areas Commun.*, vol. 3, no. 1, pp. 100–110, Jan. 1985, doi: 10.1109/JSAC.1985.1146168.

[13] D. J. Sanchez and D. W. Oesch, "The creation of angular momentum in optical waves propagating through atmospheric turbulence," in *Proc. Frontiers Opt.*, 2011, pp. 1–7, doi: 10.1364/FIO.2011.FTuY6.

[14] D. J. Sanchez and D. W. Oesch, "Localization of angular momentum in optical waves propagating through turbulence," *Opt. Express*, vol. 19, no. 25, pp. 25388–25396, Dec. 2011, doi: 10.1364/OE.19.025388.

[15] D. J. Sanchez and D. W. Oesch, "Orbital angular momentum in optical waves propagating through distributed turbulence," *Opt. Express*, vol. 19, no. 24, pp. 24596–24608, Nov. 2011, doi: 10.1364/OE.19.024596.

[16] A. Mahalov, "Multiscale modeling and nested simulations of three-dimensional ionospheric plasmas: Rayleigh–Taylor turbulence and non-equilibrium layer dynamics at fine scales," *Phys. Scripta*, vol. 89, no. 9, Sep. 2014, Art. no. 098001, doi: 10.1088/0031-8949/89/9/098001.

[17] A. Mahalov and M. Moustaoui, "Multiscale nested simulations of Rayleigh–Taylor instabilities in ionospheric flows," *J. Fluids Eng.*, vol. 136, no. 6, pp. 060908–060916, Jun. 2014, doi: 10.1115/1.4025657.

[18] W. Tang and A. Mahalov, "Stochastic lagrangian dynamics for charged flows in the E-F regions of ionosphere," *Phys. Plasmas*, vol. 20, no. 3, Mar. 2013, Art. no. 032305, doi: 10.1063/1.4794735.

[19] W. Tang and A. Mahalov, "The response of plasma density to breaking inertial gravity wave in the lower regions of ionosphere," *Phys. Plasmas*, vol. 21, no. 4, Apr. 2014, Art. no. 042901, doi: 10.1063/1.4870760.

[20] D. C. Fritts *et al.*, "The deep propagating gravity wave experiment (DEEPWAVE): An airborne and ground-based exploration of gravity wave propagation and effects from their sources throughout the lower and middle atmosphere," *Bull. Amer. Meteorol. Soc.*, vol. 97, no. 3, pp. 425–453, Mar. 2016, doi: 10.1175/BAMS-D-14-00269.1.

[21] S. T. Loi *et al.*, "Real-time imaging of density ducts between the plasmasphere and ionosphere," *Geophys. Res. Lett.*, vol. 42, no. 10, pp. 3707–3714, 2015. [Online]. Available: https://agupubs.onlinelibrary.wiley.com/doi/abs/10.1002/2015GL063699

[22] G. Spanjers *et al.*, "The AFRL demonstration and science experiments (DSX) for DoD space capability in the MEO," in *Proc. IEEE Aerosp. Conf.*, Mar. 2006, p. 10, doi: 10.1109/AERO.2006.1655750.

[23] M. Knapp *et al.*, "Hero: A space-based low frequency interferometric observatory for heliophysics enabled by novel vector sensor technology," in *Proc. 8th Int. Workshop Planet., Sol. Heliospheric Radio Emissions held at Seggauberg near*, Graz, Austria, Oct. 2016, pp. 411–424. [Online]. Available: https://www.austriaca.at/?arp=0x0039b73f

[24] C. Ferencz, "Electromagnetic wave propagation in inhomogeneous, moving media: A general solution of the problem," *Radio Sci.*, vol. 46, no. 5, pp. 1–4, Oct. 2011. [Online]. Available: https://agupubs.onlinelibrary.wiley.com/doi/abs/10.1029/2011RS004686

[25] F. Lind *et al.*, "AERO & VISTA: Demonstrating HF radio interferometry with vector sensors SSC19-WKV-09," *33rd Annu. AIAA/USU Conf. Small Satell.*, 2019, pp. 1–7.

[26] M. Knapp *et al.*, "Vector antenna and maximum likelihood imaging for radio astronomy," in *Proc. IEEE Aerosp. Conf.*, Mar. 2016, pp. 1–17, doi: 10.1109/AERO.2016.7500688.

[27] J. A. Durazo, E. J. Kostelich, and A. Mahalov, "Local ensemble transform Kalman filter for ionospheric data assimilation: Observation influence analysis during a geomagnetic storm event," *J. Geophys. Res., Space Phys.*, vol. 122, no. 9, pp. 9652–9669, Sep. 2017. [Online]. Available: https://agupubs.onlinelibrary.wiley.com/doi/abs/10.1002/2017JA024274

[28] S.-P. Moschou *et al.*, "Synthetic radio imaging for quiescent and CME-flare scenarios," *Astrophys. J.*, vol. 867, no. 1, p. 51, Oct. 2018, doi: 10.3847/1538-4357/aae58c.

[29] O. Cohen *et al.*, "Exoplanet modulation of stellar coronal radio emission," *Astronomical J.*, vol. 156, no. 5, p. 202, Oct. 2018, doi: 10.3847/1538-3881/aae1f2.

[30] S. Giacintucci, M. Markevitch, M. Johnston-Hollitt, D. R. Wik, Q. H. S. Wang, and T. E. Clarke, "Discovery of a giant radio fossil in the ophiuchus galaxy cluster," *Astrophys. J.*, vol. 891, no. 1, p. 1, Feb. 2020.
[31] Q. Wang *et al.*, "CASPER: Coupled air–sea processes and electromagnetic ducting research," *Bull. Amer. Meteorol. Soc.*, vol. 99, no. 7, pp. 1449–1471, Jul. 2018, doi: 10.1175/BAMS-D-16-0046.1.
[32] H. C. Ward, J. G. Evans, C. S. B. Grimmond, and J. Bradford, "Infrared and millimetre-wave scintillometry in the suburban environment—Part 1: Structure parameters," *Atmos. Meas. Techn.*, vol. 8, no. 3, pp. 1385–1405, Mar. 2015, doi: 10.5194/amt-8-1385-2015.
[33] H. C. Ward, J. G. Evans, and C. S. B. Grimmond, "Infrared and millimetre-wave scintillometry in the suburban environment—Part 2: Large-area sensible and latent heat fluxes," *Atmos. Meas. Techn.*, vol. 8, no. 3, pp. 1407–1424, Mar. 2015, doi: 10.5194/amt-8-1407-2015.
[34] H. C. Ward, "Scintillometry in urban and complex environments: A review," *Meas. Sci. Technol.*, vol. 28, no. 6, May 2017, Art. no. 064005, doi: 10.1088/1361-6501/aa5e85.
[35] M. Zieliáski, K. Fortuniak, W. Pawlak, and M. Siedlecki, "Long-term turbulent sensible-heat-flux measurements with a large-aperture scintillometer in the centre of, central poland," *Boundary-Layer Meteorol.*, vol. 167, no. 3, pp. 469–492, Jun. 2018, doi: 10.1007/s10546-017-0331-5.
[36] G. Pozníková *et al.*, "Quantifying turbulent energy fluxes and evapotranspiration in agricultural field conditions: A comparison of micrometeorological methods," *Agricult. Water Manage.*, vol. 209, pp. 249–263, Oct. 2018, doi: 10.1016/j.agwat.2018.07.041.
[37] A. Musa and B. S. Paul, "A review of microwave cross polarization in sand and dust storms," *J. Commun.*, vol. 14, no. 11, pp. 1026–1033, 2019, doi: 10.12720/jcm.14.11.1026-1033.
[38] M. Wagner, P. Gerstoft, and T. Rogers, "Estimating refractivity from propagation loss in turbulent media," *Radio Sci.*, vol. 51, no. 12, pp. 1876–1894, Dec. 2016, doi: 10.1002/2016RS006061.
[39] L. La Spada, S. Haq, and Y. Hao, "Modeling and design for electromagnetic surface wave devices," *Radio Sci.*, vol. 52, no. 9, pp. 1049–1057, Sep. 2017, doi: 10.1002/2017RS006379.
[40] M. Gilman, E. Smith, and S. Tsynkov, *Transionospheric Synth. aperture Imag*. Cham, Switzerland: Springer, 2017, doi: 10.1007/978-3-319-52127-5.
[41] S. G. Lee, S. W. Ra, and S. J. Lee, "Depolarization mitigation using frequency offset in the dual-polarized X-band for eess," in *Proc. Int. Workshop Satell. Space Commun.*, Sep. 2006, pp. 25–28, doi: 10.1109/IWSSC.2006.255983.
[42] V. A. Sinclair, D. Moisseev, and A. von Lerber, "How dual-polarization radar observations can be used to verify model representation of secondary ice," *J. Geophys. Res., Atmos.*, vol. 121, no. 18, pp. 10954–10970, 2016, doi: 10.1002/2016JD025381.
[43] A. Taflove and S. C. Hagness, *Computational Electrodynamcis—The Finite-Difference Time-Domain Method*, 3rd ed. Norwood, MA, USA: Artech House, 2005.
[44] C. Wang and T. Keech, "Antenna models for electromagnetic compatibility analyses," U.S. Dept. Commerce, Nat. Telecommun. Inf. Admin., Boston, MA, USA, Tech. Rep. TM-13-489, Oct. 2012.
[45] Q. Wang *et al.*, "Range and height measurement of X-band EM propagation in the marine atmospheric boundary layer," *IEEE Trans. Antennas Propag.*, vol. 67, no. 4, pp. 2063–2073, Apr. 2019, doi: 10.1109/TAP.2019.2894269.
[46] M. Ulate, Q. Wang, T. Haack, T. Holt, and D. P. Alappattu, "Mean offshore refractive conditions during the CASPER east field campaign," *J. Appl. Meteorol. Climatol.*, vol. 58, no. 4, pp. 853–874, Apr. 2019.
[47] J. E. Chamberlain, F. D. Findlay, and H. A. Gebbie, "Refractive index of air at 0.337-mm wave-length," *Nature*, vol. 206, no. 4987, pp. 886–887, May 1965, doi: 10.1038/206886a0.
[48] J.-P. Berenger, "A perfectly matched layer for the absorption of electromagnetic waves," *J. Comput. Phys.*, vol. 114, no. 2, pp. 185–200, Oct. 1994, doi: 10.1006/jcph.1994.1159.
[49] K. Yee, "Numerical solution of initial boundary value problems involving Maxwell's equations in isotropic media," *IEEE Trans. Antennas Propag.*, vol. 14, no. 3, pp. 302–307, May 1966, doi: 10.1109/TAP.1966.1138693.
[50] D. C. Cox, "Depolarization of radio waves by atmospheric hydrometeors in Earth-space paths: A review," *Radio Sci.*, vol. 16, no. 5, pp. 781–812, Sep. 1981, doi: 10.1029/RS016i005p00781.

Stephen R. Shaffer received the B.S. degree in astronomy, physics, and mathematics from the University of Arizona, Tucson, AZ, USA, in 2005, the M.S. and Ph.D. degrees in mechanical engineering from Arizona State University, Tempe, AZ, USA, in 2009 and 2014, respectively. His dissertation was on investigations of environmental effects on freeway acoustics.

He held a post-doctoral position with the School of Mathematical and Statistical Sciences, Arizona State University, from 2014 to 2019, where he is currently an Assistant Research Professor.

Alex Mahalov received the Ph.D. degree in applied mathematics from Cornell University, Ithaca, NY, USA, in 1991.

He held a post-doctoral position with the Department of Mechanical Engineering, University of California at Berkeley, Berkeley, CA, USA. He joined Arizona State University, Tempe, AZ, USA, where he was promoted to the Wilhoit Foundation Deans Distinguished Professor in 2008. He has authored over 150 research articles and scientific reports. His current research interests include the stochastic Maxwell equations and their applications, computational modeling, imaging, optical turbulence, and the stochastic theory of electromagnetic wave propagation.